Pulsed high magnetic field sensor using polymethyl methacrylate



2006 Meas. Sci. Technol. 17 2015

(http://iopscience.iop.org/0957-0233/17/7/047)

INSTITUTE OF PHYSICS PUBLISHING MEASUREMENT SCIENCE AND TECHNOLOGY

Meas. Sci. Technol. **17** (2006) 2015–2021 doi:10.1088/0957-0233/17/7/047

# Pulsed high magnetic field sensor using polymethyl methacrylate

**Eul Ha Hwang and Byoung Yoon Kim**

Department of Physics, Korea Advanced Institute of Science and Technology, 373-1, Kuseong-dong, Yusong-gu, Taejon 305-701, Korea

E-mail: ehwang@kaist.ac.kr and yoonkim@kaist.ac.kr

Received 9 March 2006, in final form 13 May 2006
Published 21 June 2006
Online at stacks.iop.org/MST/17/2015

**Abstract**

We propose and demonstrate the use of polymethyl methacrylate (PMMA) for sensing elements based on the Faraday effect for the measurement of a pulsed high magnetic field generated by helical magnetic flux compression generators (HMCGs). The magneto-optic properties of sensing elements made with PMMA are investigated. The inherent linear birefringence is substantially suppressed by carefully annealing PMMA blocks. The Verdet constant of $V = 3.251\,\mathrm{rad\,T^{-1}\,m^{-1}}$ and the normalized temperature dependence of $VL$ (the product of the Verdet constant and the length of the sensing element) of $-2.04 \times 10^{-4}\,^{\circ}\mathrm{C}^{-1}$ are measured in the annealed PMMA material. The pulsed high magnetic field of up to ∼27 kG is measured by the sensors made from annealed PMMA and the results are compared with those measured by inductive probes. They are in good agreement within ±1.5%. As an application, the annealed PMMA sensor is used in the measurement of a pulsed magnetic field generated by explosive-driven HMCGs.

**Keywords:** polymethyl methacrylate, Faraday rotation, linear birefringence, Verdet constant, explosive

## 1. Introduction

The time history of compressed magnetic flux density generated from helical magnetic flux compression generators (HMCGs) driven by high explosive (HE) is one of the most important parameters in evaluating the performance of HMCGs and for redesigning them [1]. In order to avoid problems associated with electromagnetic interference (EMI) and electrical insulation, optical sensors based on the Faraday effect have been preferred for the measurement of the compressed magnetic flux densities generated by HMCGs [2–7]. Since the magnitude of the magnetic field of interest is very high (in the order of Tesla), quartz glass plates or rods with small dimensions (of the order of 1 cm) have been used as the sensor heads [2, 4, 6]. This results in a simpler sensor construction compared to all-fibre-optic sensors that require precise control of fibre alignment and polarization state of light in the optical fibre, along with the suppression of mechanical vibration of the system [8, 9]. Also, the use of special material with large Verdet constant [10, 11] is not needed for the application. The Verdet constant of quartz glass material shows low temperature dependence and low hysteresis.

In the practical testing environment of HMCGs, however, a low cost sensor material that is easy to manipulate in the field to form different shapes and sizes is desirable. This is because the sensor heads sometimes need to be positioned at different places in the HMCG on sites that are completely destroyed after the test. Plastic material would be a good candidate for the purpose with its easy machinability and low cost.

In this paper, we propose and characterize in detail, for the first time to our knowledge, a magnetic field sensor for HMCG made of bulk PMMA (polymethyl methacrylate manufactured by polycast Technology Corporation). The Verdet constant of PMMA was measured to be comparable to that of quartz glass, and inherent birefringence in the sensor head could be suppressed by an annealing process. We demonstrate its application to the measurement of the time history of a pulsed high magnetic field generated by a small scale HMCG. We compare the results of the magnetic

  

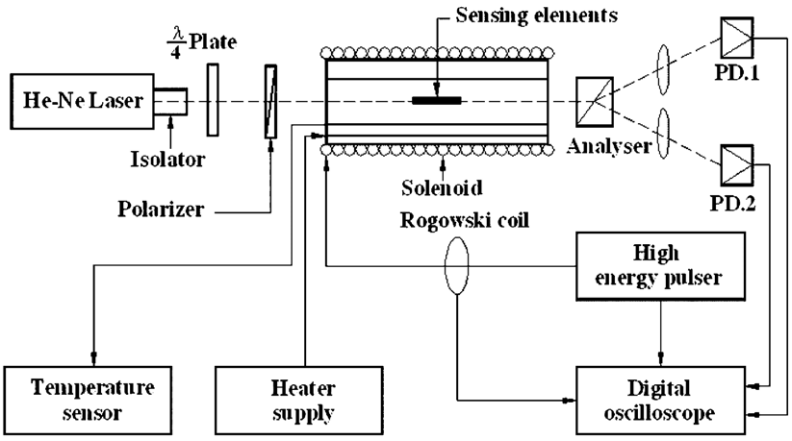


**Figure 1.** The block diagram of the system for measuring the optical properties of a sensing element. PD.1, PD.2: PIN silicon photo detectors. Dashed lines and solid lines represent laser beam and electric wire, respectively.

field measurement with the results obtained with FRG-04 (crystaltechno LDT) glass used as a reference sensing material, and show that PMMA sensors could be used for the measurement of the time history of a pulsed high magnetic field.

## 2. Characterization of PMMA for magnetic field sensing

### *2.1. Experimental setup and measurement principle*

Figure 1 shows the schematic of an experimental setup used to measure the inherent linear birefringence and the $VL$ (the product of Verdet constant $V$ and length $L$) of PMMA material as a function of temperature. The PMMA samples were prepared by cutting a 1″ thick plate into cylindrical shapes of 1″ diameter. Linearly polarized light from an intensity-stabilized He–Ne laser travels through a $\lambda/4$ plate and then a rotatable linear polarizer. The orientation of the $\lambda/4$ plate was at $\pm 45^\circ$ with respect to the polarization plane of the He–Ne laser beam so that the light after the $\lambda/4$ plate was circularly polarized. The linearly polarized light incident on a sensing element had a constant intensity regardless of the orientation of the polarizer angle. The light beam emerging from a sensing element was split into two orthogonal polarization components by a Wollaston analyser, and their intensities $(I_1, I_2)$ were measured by two photodetectors (PD.1, PD.2) and recorded using a digital oscilloscope. The surface temperature of the sensing element was varied by heating the solenoid coil, and measured by a K-type thermocouple in contact with the surface of the sensing element.

Our measurement for the linear birefringence of sensing element is based on the linear retarder model [12]. The inherent linear birefringence degrades the sensitivity and accuracy of the magnetic field induced circular birefringence, and therefore should be suppressed. If the analyser and the two photo-detectors are rotated in unison so that the function $P(\theta_0) = \frac{(I_1 - I_2)}{(I_1 + I_2)}$ reaches a maximum value $P_{\max}(\theta_0) = \frac{(I_{1\max} - I_{2\min})}{(I_{1\max} + I_{2\min})}$ for a given input polarization angle $\theta_0$, then $P_{\max}(\theta_0)$ is represented by

$$P_{\max}(\theta_0) = \sqrt{\cos^2(2\theta_0) + \sin^2(2\theta_0)\cos^2(\delta)}. \tag{1}$$

Here, $\theta_0$ is the angle between the input linear polarization and the birefringence axis of the sample, and $\delta$ is the phase retardation due to the linear birefringence, $I_{1\max}$ and $I_{2\min}$ are the maximum intensity measured by PD.1 and the minimum intensity measured by PD.2, respectively. Therefore, the magnitude of $\delta$ can be determined by measuring $P_{\max}(\theta_0)$ as a function of $\theta_0$ using equation (1).

When an external magnetic field $B$ is applied to a sensing element having no inherent birefringence, circular birefringence is induced that rotates the direction of input linear polarization (known as the Faraday rotation) by an angle

$$\theta_F = V \int_L \vec{B} \cdot \mathrm{d}\vec{L} = VBL.$$

Here, $V$ is the Verdet constant and $L$ is the length of the sample. In this case, if we use the setup in figure 1 with the polarization angle of the Wollaston analyser at $\pm 45^\circ$ with respect to that of the input polarizer, the magnetic field $B$ can be determined from

$$P = \frac{I_1 - I_2}{I_1 + I_2} = \sin(2\theta_F). \tag{2}$$

In the presence of inherent linear birefringence with the total phase retardation $\delta$, and the input polarization angle $\theta_0 = 0$, we obtain [12–15]

$$P(0) = \frac{I_1 - I_2}{I_1 + I_2} = \frac{2\theta_F \sin\phi}{\phi}, \tag{3}$$

where

$$\phi^2 = \delta^2 + (2\theta_F)^2. \tag{4}$$

For two extreme cases of $\delta \ll 2\theta_F$ and $2\theta_F \ll \delta$, equation (3) can be approximated as the following equations (5) and (6), respectively:

$$P(0) \approx \sin(2\theta_F), \tag{5}$$

$$P(0) \approx 2\theta_F \frac{\sin\delta}{\delta}. \tag{6}$$

For the case of $\phi \ll 1$ (e.g., $\delta \ll 1$ and $\theta_F \ll 1$), equations of (3), (5) and (6) can be simplified as in equation (7):

$$P(0) \approx 2\theta_F. \tag{7}$$

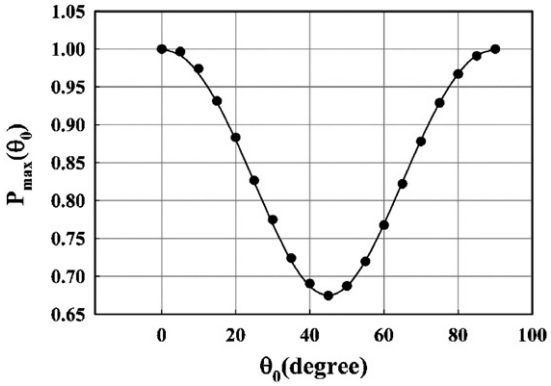


**Figure 2.** Measured values of $P_{\max}$ as a function of $\theta_0$ for unannealed PMMA (length $L$= 24.84 mm) at room temperature. The line shows the result calculated from equation (1).

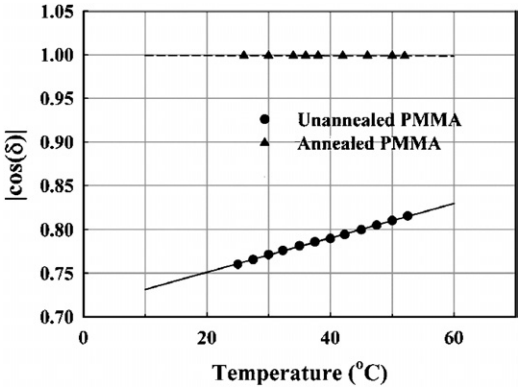


**Figure 3.** Relations between $|\cos\delta|$ and temperature in PMMA materials (manufactured by polycast Technology Corporation). The lines in the figure are linear fits.

In the case of $\delta \ll 2\theta_F$, the measurement becomes straightforward since it is independent of the total retardation in the sensing head. However, in the case of $2\theta_F \ll \delta$, the output $P(0)$ sensitively depends on the phase retardation $\delta$, and therefore reduces the practicality of the sensor. Therefore, the criteria for $\delta$ should be $\delta \ll 1$, in which case equation (6) also becomes independent of $\delta$. Since the parameters such as $V$, $L$ and $\delta$ are temperature dependent, it is necessary to examine the effects of temperature on $VL$ and $\delta$ for the sensing elements.

### *2.2. Measurement of inherent birefringence and its temperature dependence*

Figure 2 shows experimental results of $P_{\max}(\theta_0)$ for an unannealed PMMA sample. As shown in the figure, the measured data agree well with a curve generated by equation (1) based on the linear retarder model. This sample clearly shows the existence of linear birefringence and the origin is considered to be the residual stresses in the material. Since $P_{\max}(\theta_0) = |\cos\delta|$ at $\theta_0 = 45^\circ$ from equation (1), the room temperature retardance of this sample was estimated to be $\delta \approx 0.83$ rad from the data of figure 2, and that does not satisfy the desired condition $\delta \ll 1$.

Under the magnetic field (∼4.2 kG) generated by the setup in figure 1 for the calibration of the sensor, the induced circular birefringence $\theta_F$ of the PMMA materials (1″ in length) is estimated to be about $3.5 \times 10^{-2}$ rad, and therefore, the approximation in equation (6) applies. In this case, the value of $\frac{\sin\delta}{\delta}$ is ∼0.89, which can lead to an error of ∼11.0% if the dependence on $\delta$ is not taken into account. This is too large compared to our target error limit for the magnetic field sensor of 3%. The magnetic field typically generated by an actual HMCG is on the order of 100 kG, which corresponds to $\theta_F$ of ∼0.78 rad that is comparable to the inherent retardation in the sample. This makes the measurement of the magnetic field non-trivial with a simple setup. Therefore, it is necessary to suppress the inherent birefringence in the sensing material.

In order to suppress the inherent linear birefringence of PMMA material, the sample was annealed in air by using an automatic temperature controlled oven for 48 h. The temperature of the oven was raised to 80 °C at the rate of 20 °C $h^{-1}$, held at the maximum temperature for 8 h, and cooled until it reached room temperature at the rate of 1.6 °C $h^{-1}$. Using the annealed sample, we measured the temperature dependence of $\delta$, and compared it with that of an unannealed sample. Figure 3 shows the measured values of $P_{\max}(\theta_0 = 45^\circ) = |\cos\delta|$ for the annealed ($L = 25.4$ mm) and the unannealed ($L = 24.84$ mm) PMMA samples as a function of temperature. The phase retardations can be readily obtained from data in figure 3, and the results are plotted in figure 4. By annealing the PMMA material, its room temperature phase retardation was reduced to $\delta = 0.05$ rad. Since our calibration measurement produces $2\theta_F = 0.07$ rad, the condition $\phi \ll 1$ is satisfied and equation (7) can be applied. This approximation results in the error of ∼0.04% compared to equation (3) which is acceptable. The phase retardation $\delta$ remained below ∼0.05 rad for the annealed sample for the temperature range of 20–60 °C. The first-order coefficient of the fitted curve for $\delta(T)$ was $d\delta/dT = 2.24 \times 10^{-4}$ rad °$C^{-1}$ for annealed PMMA and $d\delta/dT = -32.03 \times 10^{-4}$ rad °$C^{-1}$ for unannealed PMMA. These results show that the annealing reduces the inherent linear birefringence and its temperature dependence sufficiently for practical application to measuring large magnetic field generated by HMCGs.

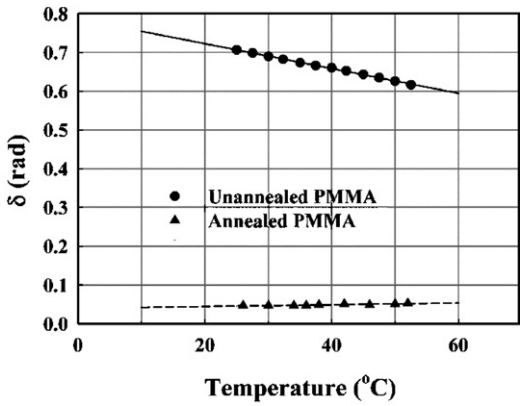


**Figure 4.** Temperature dependence of $\delta$ in PMMA samples. The lines in the figure are linear fits.

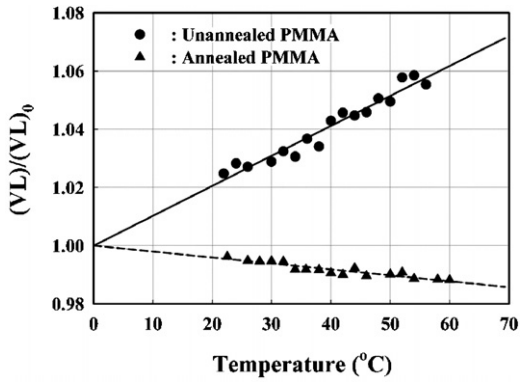


**Figure 5.** Normalized temperature responses of $VL$ in PMMA material. The lines in the figure are linear fits. $(VL)_0$: the value of $(VL)$ at 0 °C.

**Table 1.** Results for PMMA material and glasses.

| Material | $V_{20\,^\circ\mathrm{C}}$ (rad T$^{-1}$ m$^{-1}$) | $\frac{1}{(VL)_0}[\frac{\mathrm{d}(VL)}{\mathrm{d}T}]$ ($10^{-4}$ °C$^{-1}$) |
|---|---|---|
| Annealed PMMA | 3.251 ± 0.002 | −2.040 ± 0.000 |
| Unannealed PMMA | 3.122 ± 0.004 | +9.770 ± 0.530 |
| Fused quartz | 3.663[2], 3.678 | +0.089 |
| FRG-04 glass | −73.807[10] | – |

### *2.3. Verdet constant and its temperature dependence*

In order to measure the Verdet constant and the temperature dependence of $VL$, the sensing element was subjected to an applied magnetic field (∼2.4 kG) generated by a single layer solenoid (46.2 mm in diameter, 485 mm in length, 572 turns) and a capacitor of 8 $\mu$F charged to 4.50 kV. The electric current of a solenoid coil was measured by a commercial inductive probe (Pearson Electronics Inc., Model: 101). Figure 5 shows the temperature dependence of $(VL)$ normalized to its 0 °C value $(VL)_0$ for the annealed and unannealed PMMA. The data of $VL$ were obtained by using the approximation (6) and (7) for unannealed PMMA and annealed PMMA, respectively.

By increasing the temperature from 20 °C to 60 °C, the value of $(VL)/(VL)_0$ increased by ∼4.10% for an unannealed PMMA, which is beyond our target error level. On the other hand, the annealed PMMA material shows the variation of $(VL)/(VL)_0$ within ∼1.18% as shown in figure 5. For comparison, we measured the values and the temperature dependence of $(VL)/(VL)_0$ for four different materials, and the results are summarized in table 1. The data for PMMA material represent the averages of ten measurements.

Since the hystereisis in the response to the magnetic field can affect the measurement, we measured $P(0)$ as we vary the applied magnetic field between −10 kG and 27 kG. The results are shown in figure 6, and there was no evidence of hysteresis. Here, the applied magnetic field and $P(0)$ were measured by an inductive probe (Pearson Electronics Co., Model 101) and the annealed PMMA sensor. The magnetic fields measured by these two sensors were in good agreement within 1.5%.

We compared our experimental results with calculations based on the method [16–18] which is used to estimate the Verdet constant of optical media from molar ionic Verdet constants. The calculation yielded a Verdet constant of unannealed PMMA of about 2.647 rad T$^{-1}$ m$^{-1}$ at room temperature (300 K) and at $\lambda = 633$ nm. This is about 15% less than our experimental value and is in reasonably good agreement.

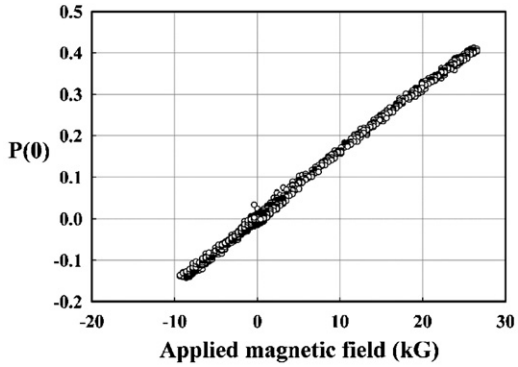


**Figure 6.** Magneto-optic response of annealed PMMA material.

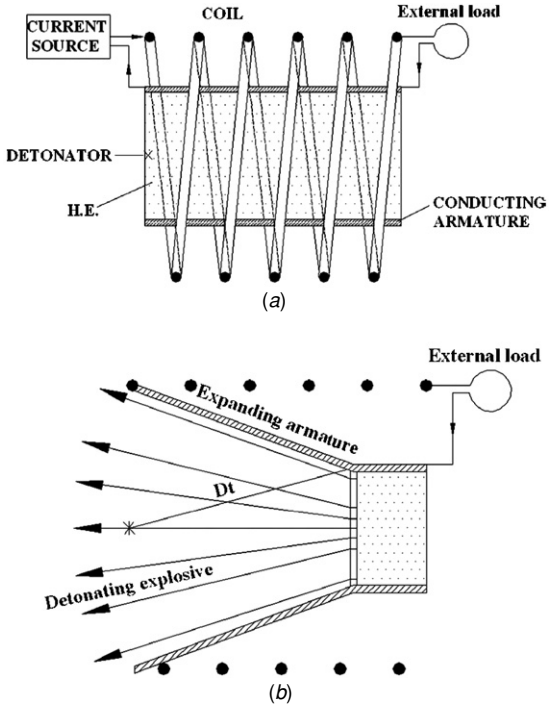


**Figure 7.** Configuration of HMCG. (*a*) Before initiating a detonator; (*b*) after initiating a detonator; H.E.: high explosive. Diameter of external load: 40 mm.

## 3. Measurement of the pulsed magnetic field generated by a HMCG

### *3.1. Configuration of HMCG*

The HMCG is an explosive device to convert the chemical energy of high explosive into the electromagnetic energy. As shown in figure 7, a HMCG consists of a cylindrical conducting armature filled with high explosive, a multi turn coaxial helix of enamelled wires and a single turn copper external load [19]. A capacitor bank is connected to the solenoid coil and conducting armature, and supplies the initial energy to the system.

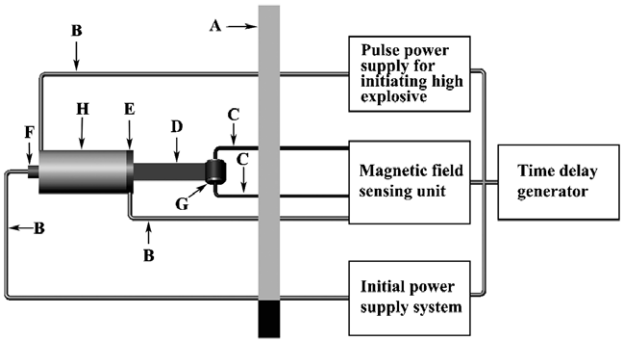


**Figure 8.** The experimental setup for HMCG tests. A: bunker wall; B: electric lines; C: multi-mode optical fibre (MMF); D: external load; E: Rogowski current sensor; F: detonator; G: PMMA sensor head; H: HMCG.

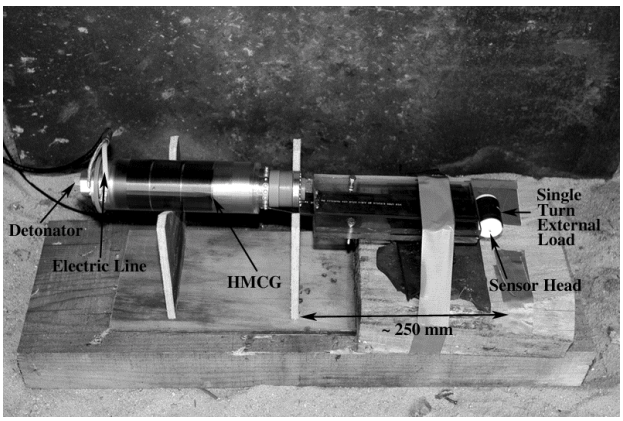


**Figure 9.** A photograph of the HMCG system.

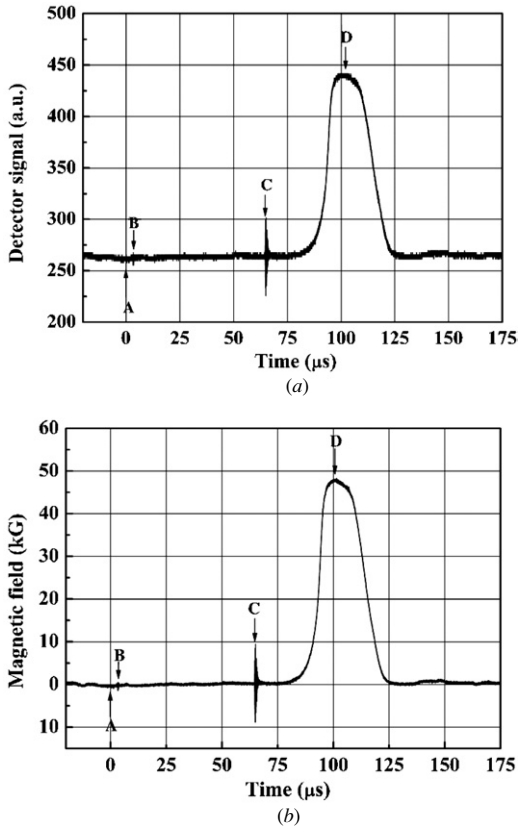


**Figure 10.** Signals measured by the annealed PMMA Faraday rotator in the HMCG test. (*a*) Light intensity measured by a photo detector; (*b*) magnetic field intensity obtained by a signal process; A: trigger point for capacitor bank; B: operating point of spark gap switch; C: initiating point of a detonator and D: peak point of signal.

The cylindrical armature driven by the detonating explosive expands like a cone whose wall contacts the helix as shown in figure 7(*b*). As the detonation propagates, the contact point moves along the axis of the solenoid, and consequently the inductance of the closed circuit decreases as a function of time. As a result, the exploding armature compresses magnetic flux and amplifies the current supplied initially by a capacitor bank.

### *3.2. Measurement of the pulsed magnetic field compressed by the HMCG*

The overall experimental setup for the HMCG test is sketched in figure 8. The fabricated HMCG consists of a cylindrical conducting armature filled with about 100 g of high explosive and a single turn copper external load (44.5 mm in width, 1.2 mm in thickness and 40 mm in diameter).

The external load is enclosed in a heat shrinking tube (Ace Tube®, size 38 mm, LR103775) to provide enough insulation between two lead strips. The single turn external load is separated from the HMCG by about 250 mm to protect the optical fibre and the sensor head imbedded in the external load from the shock wave generated by the high explosive. Some baffle-boards are also mounted between an optical sensor head and the HMCG. Figure 9 shows a picture of the HMCG system with an external load and an optical sensor head.

In order to measure the magnetic field along the central axis of the external load, a 20 mW laser diode (LD) ($\lambda$ = 635 nm) is used as the light source for the annealed PMMA Faraday rotator (15 mm in diameter, 24 mm in length). The core diameter and length of a multi-mode fibre (MMF) are 200 $\pm$ 8 $\mu$m and 20 m, respectively. The polarization-foils (hama® 4810) of 0.4 mm in thickness glued onto both end surfaces of the sensing element are used as the polarizer and the analyser. The polarization axis of analyser is set to 45° with respect to that of a polarizer for maximum sensitivity. The light beam emitted from the light source is launched into the core of MMF using a microscope objective lens (Olympus M40). The light beam emerging from the MMF is converted into linearly polarized light with a constant intensity by the polarizer and collimated by a BK-7 rod lens of 4 mm in diameter and 5 mm in length (TECH SPEC). This collimated light beam passes through the sensor head (consisting of the polarizer, the Faraday rotator and the analyser). The light beam after the analyser is focused on the core of MMF by another BK-7 rod lens, and transmitted to a photo detector (THORABS Inc. Model: DET110). Also, in another experiment, a FRG-04 glass (15 mm in diameter and length) having $V$ = $-73.8$ rad T$^{-1}$ m$^{-1}$ is used as a reference sensor for the calibration of an annealed PMMA Faraday rotation sensor. Since the field-induced circular birefringence in the HMCG test is much larger than the linear birefringence of these two

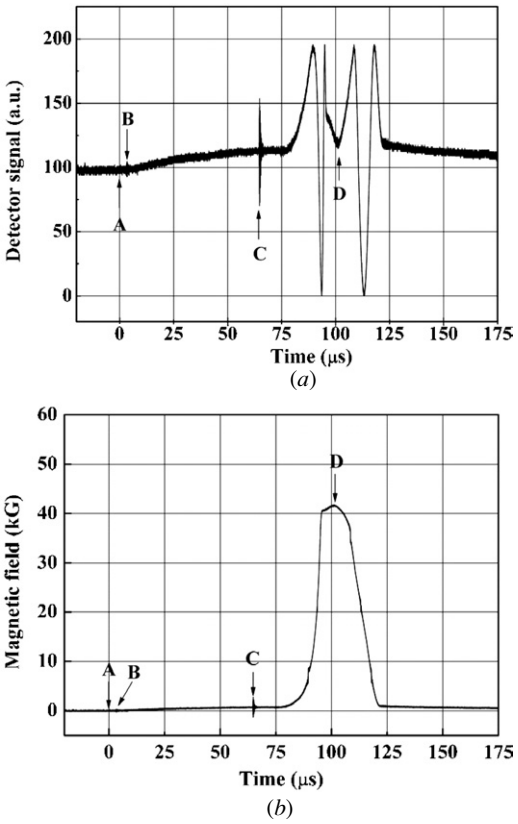


**Figure 11.** Signals measured by a FRG-04 Faraday rotator in the HMCG test. (*a*) Signal recorded by a photo detector; (*b*) magnetic field intensity obtained by a signal process.

sensing elements, errors due to the linear birefringence of sensing elements can be neglected, and thus, the normalized light intensity ($I$) measured in HMCG tests can be expressed by

$$I = \tfrac{1}{2}[1 + \sin(2\theta_{\mathrm{F}})]. \tag{8}$$

Therefore, the field-induced circular birefringence $\theta_{\mathrm{F}}$ can be obtained from (8), and the magnetic field also can be easily obtained by $B = \theta_{\mathrm{F}}/VL$.

In the first field shot of HMCG, the signal shown in figure 10 was obtained from an annealed PMMA Faraday rotating sensor.

In order to compare an annealed PMMA Faraday rotator with a reference Faraday rotator, a FRG-04 glass was used as a standard Faraday rotator in the second field shot, and the result is shown in figure 11. As compared with FRG-04 glass, the Verdet constant of annealed PMMA was about 23 times less than that of FRG-04 glass, but the magnetic field profile measured by the annealed PMMA sensor agrees very well with that by FRG-04 glass as shown in figures 10(*b*) and 11(*b*). Because these two results were obtained from the different events of the HMCG test, the peak values of magnetic field showed slightly different values.

In figures 10 and 11, point A represents the initial trigger (0 $\mu$s) of a time delay generator. The spark gap switch of capacitor is triggered at the position B (∼3.3 $\mu$s), and a capacitor (∼50 $\mu$F) charged to 4.5 kV is simultaneously discharged. When the initial current of the closed circuit formed by helical coil and external load reaches the maximum value, the detonator of figure 7(*a*) is initiated at the position C (∼65 $\mu$s). The magnetic field compressed by the expanding armature reaches the maximum value at the position D (∼ 101 $\mu$s). In the second shot, the peak value of initial magnetic field was measured to be ∼0.7 kG, and the peak value of magnetic field compressed by the small HMCG was measured to be 41.8 kG. On the other hand, in the first shot with the annealed PMMA sensor, the signal of the initial magnetic field (e.g., position C of figure 10(*a*)) was too small to measure, and the peak value of compressed magnetic field was measured to be 48.2 kG. The reason for this small signal of the initial magnetic field is that the Verdet constant of the annealed PMMA sensor is about 23 times less than that of FRG-04 glass. However, the compressed high magnetic field measured by the annealed PMMA sensor showed the same time history as that by FRG-04 glass.

## 4. Conclusions

The use of polymethyl methacrylate as the sensing element based on the Faraday effect for the measurement of a pulsed high magnetic field has been proposed and demonstrated. The inherent linear birefringence has been suppressed by the annealing process, and their optical characteristics have also been examined and discussed. The magnetic fields measured by both the PMMA sensor and the inductive probe are in good agreement within ±1.5% under a pulsed high magnetic field of up to ∼27 kG. The measurement of the high pulsed magnetic field (∼45 kG) compressed by the explosive-driven HMCG has been demonstrated by using the annealed PMMA sensor. The PMMA sensor can be practically used for the measurement of a high magnetic field generated by HMCGs with less than 3% measurement error.

## References

[1] Turchi P J 1980 *Megagauss Physics and Technology* (New York: Plenum) pp 1–46, pp 163–218
[2] Garn W B, Caird R S, Fowler C M and Thomson D B 1968 Measurement of Faraday rotation in megagauss fields over the continuous visible spectrum *Rev. Sci. Instrum.* **39** 1313–7
[3] Massey G A, Erickson D C and Kadlec R A 1975 Electromagnetic field components: their measurement using linear electrooptic and magnetooptic effects *Appl. Opt.* **14** 2712–9
[4] Smeulders P J 1976 Field measurements in a pinch discharge using magneto-optical probe *J. Phys. D: Appl. Phys.* **9** 413–21
[5] Lassing H, Mastop W, van der Meer A and Oomens A 1987 Plasma current measurements by Faraday rotation in a single-mode fiber *Appl. Opt.* **26** 2456–60
[6] Novac B M, Smith I R, Stewardson H R and Senior P 1996 Experimental methods with flux-compression generator *IEEE Eng. Sci. Educ. J.* **5** 211–22
[7] Forman P R and Jahoda F C 1988 Linear birefringence effects on fiber-optic current sensors *Appl. Opt.* **27** 3088–96
[8] Akira E, Masayuki I and Tadasi S 1987 Optical fiber sensors using the method of polarization-rotated reflection *J. Lightwave Technol.* **5** 1584–90
[9] Fang X, Wang A, May R G and Claus R O 1994 A reciprocal-compensated fiber-optic electric current sensor *J. Lightwave Technol.* **12** 1882–90

[10] Datasheet of crystaltechno LDT. (www.crystaltechno.com)
[11] Optical Glass, Shott Optical Glass, Inc. (www.Shottglasstech.com)
[12] Smith A M 1978 Polarization and magnetooptic properties of single-mode optical fiber *Appl. Opt.* **17** 52–6
[13] Papp A and Harms H 1975 Polarization optics of index-gradient optical waveguide fibers *Appl. Opt.* **14** 2406–11
[14] Harms H, Papp A and Kempter K 1976 Magnetooptical properties of index-gradient optical fibers *Appl. Opt.* **15** 799–01
[15] Huard S 1997 *Polarization of Light* (New York: Wiley) pp 86–131
[16] Kaminsky W and Haussühl S 1993 Anisotropy of the Faraday effect in non-cubic crystals *Z. Kristallogr.* **203** 79–91
[17] Kaminsky W 2000 Experimental and phenomenological aspects of circular birefringence and related properties in transparent crystals *Rep. Prog. Phys.* **63** 1575–640
[18] Haussühl S and Effgen W 1988 Faraday effect in cubic crystals *Z. Kristallogr.* **183** 153–74
[19] Turchi P J 1980 *Megagauss Physics and Technology* (New York: Plenum) pp 249–85